ADVANCED ENERGY MATERIALS
www.advenergymat.de

Tailoring the Cation Lattice for Chloride Lithium-Ion Conductors

*Yunsheng Liu, Shuo Wang, Adelaide M. Nolan, Chen Ling, and Yifei Mo**

All-solid-state Li-ion batteries require Li-ion conductors as solid electrolytes (SEs). Li-containing halides are emerging as a promising class of lithium-ion conductors with good electrochemical stability and other properties needed for SEs in all-solid-state batteries. Compared to oxides and sulfides, Li-ion diffusion mechanisms in Li-containing halides are less well understood, in particular regarding the effects of Li content and cation sublattices, which can be tailored for improving Li-ion conduction. Using first-principles computation, a systematic study is performed on the Li-ion conduction of known Li-containing chlorides with close-packed anion frameworks and a wide range of their doped compounds. A dozen potential chloride Li-ion conductors are predicted with increased Li-ion conductivities, and it is revealed that the Li-ion migration is greatly impacted by the cation configuration and concentrations. By analyzing a large set of materials data, it is proposed that low Li content, low cation concentration, and sparse cation distribution increase Li-ion conduction in chlorides, and these principles are demonstrated in designing new chloride Li-ion conductors. This study provides insights into the effects of the cation sublattice on Li-ion diffusion, highlights potential chloride Li superionic conductors, and proposes design principles to further develop halide Li-ion conductors.

1. Introduction

The all-solid-state Li-ion battery (ASSLB) is regarded as a key emerging rechargeable-battery technology with potential advantages over current Li-ion batteries including improved safety and higher energy density.[1–6] Solid electrolyte (SE) materials, which replace the liquid electrolyte in current Li-ion batteries, are critical for enabling ASSLBs. SE materials are lithium superionic conductors (SICs) with Li-ion conductivities >1 mS cm^{-1} at room temperature (RT), comparable to those of liquid electrolytes.[1,7,8] Only a limited number of materials systems have been demonstrated as Li SICs, including $Li_{10}GeP_2S_{12}$ (LGPS),[4] garnet $Li_7La_3Zr_2O_{12}$ (LLZO),[9,10] and NASICON $Li_{1.3}Al_{0.3}Ti_{1.7}(PO_4)_3$ (LATP).[11] However, these Li SICs do not have all properties required for ASSLBs. Compared to oxide SICs, sulfide SICs have desired mechanical deformability for forming good interface physical contacts in ASSLB cell assembly, but have narrow electrochemical window,[12,13] poor cathode interface compatibility,[14–16] and poor air/moisture stability,[5,17] which impede the large-scale commercialization of sulfide-based ASSLBs. Asano et al. discovered Li_3YCl_6 (LYC) and Li_3YBr_6 (LYB) as new Li SICs with high Li-ion conductivities on the order of 1 mS cm^{-1} at RT and with good ASSLB cell performances.[18] In addition to the desired deformable mechanical properties as sulfides, first-principles computation studies[17,19] confirmed that the chloride chemistry in general gives a lower barrier for Li-ion migration, wider electrochemical window, good interface compatibility with cathode, and good air/moisture stability compared to sulfide SEs. With a combination of multiple desired properties, lithium halides, particularly chlorides, are a promising class of Li SICs for SEs in ASSLBs.

The chloride anion chemistry is advantageous for Li-ion migration, thanks to the relatively large anion radius, large anion polarizability, and weak interaction with Li-ion.[18–20] First-principles computation confirms that Li-ion migration exhibits a low energy barrier of 0.28 eV in face-centered cubic (fcc) and of 0.29 eV in hexagonal close packed (hcp) Cl^- anion sublattices with no cation under typical lattice volume of lithium chlorides.[19] Recent experimental studies reported a series of Li-containing chlorides Li_3MCl_6 (M = In, Er, Sc) and their doped variations that achieved Li-ion conductivities on the order of 1 mS cm^{-1} at RT.[19,21–25] While the discovery of new SIC systems in oxides and sulfides is greatly limited by the unique crystal structures required for achieving fast Li-ion conduction,[26–28] Li-containing chlorides with common fcc and hcp anion sublattices exhibit adequately low Li-ion migration barrier, and are a promising chemical space for new Li-ion conductors.

A systematic fundamental understanding of chloride Li-ion conductors is essential for guiding the discovery and design new Li-containing chloride SICs. While Li-containing chlorides are common in close-packed fcc and hcp anion sublattices, they

Y. Liu, S. Wang, A. M. Nolan, Prof. Y. Mo
Department of Materials Science and Engineering
University of Maryland
College Park, MD 20742, USA
E-mail: yfmo@umd.edu
Dr. C. Ling
Toyota Research Institute of North America
Ann Arbor, MI 48105, USA
Prof. Y. Mo
Maryland Energy Innovation Institute
University of Maryland
College Park, MD 20742, USA
The ORCID identification number(s) for the author(s) of this article can be found under https://doi.org/10.1002/aenm.202002356.

DOI: 10.1002/aenm.202002356

exhibit a range of compositions with different Li/cation configurations, which have significant effects on ion conduction. For example, some earlier studied Li-containing chlorides, such as Li_2CdCl_4 and Li_2MgCl_4, were reported to have low Li-ion conductivities on the order of 10^{-6} S cm^{-1} at RT,[29–32] though these chlorides have the same close-packed fcc or hcp anion frameworks as Li_3MCl_6 (M = In, Er, Sc) SICs. Earlier reports of Li_3InCl_6 and Li_3YCl_6 also show much lower Li-ion conductivity on the order of 10^{-5} S cm^{-1}, than recent measurements with the same composition on the order of 10^{-3} S cm^{-1}.[18,21,33] It is not understood why different configurations and concentrations of Li/metal cations in Li_2MCl_4 (M = Cd, Mg) exhibit much lower ion conductivities than newly reported Li_3MCl_6 (M = In, Er, Sc) SIC systems with the same anion sublattice. In addition, doping and substitutions on these chloride SICs to tune Li concentration and cation concentration were demonstrated to further improve ionic conductivities.[22–25] It is not clear why certain doping strategies lead to improved Li-ion conductivity. To rationally guide future materials design of new halide Li-ion conductors, a scientific understanding about the effects of cation concentration, cation configuration, and Li concentration on Li-ion conduction is needed.

First-principles computation studies have led to significant progresses in understanding Li-ion diffusion mechanisms and in designing and predicting new SIC materials.[20,26,28,34,35] In this study, we perform a systematic first-principles computational study on lithium metal chloride systems spanning a wide range of Li/cation concentrations and configurations to understand the key factors determining fast Li-ion diffusion in these chloride systems. Using first-principles calculations, we study Li-ion diffusion in over 70 Li-containing chlorides from the Inorganic Crystal Structure Database (ICSD) and identify 19 materials as potential Li-ion conductors. By analyzing a large set of computation data generated on a wide range of chloride materials with different levels of doping, our computation reveals that cation configurations and Li contents significantly affect the Li-ion conductivity of chloride materials. From this understanding, we propose design principles that sparse cation configuration, low cation concentration, and low Li content increase ionic conductivity in Li-containing chlorides. Following these design principles, we artificially modify the cation lattice in a few poor Li-ion conductors and achieve increased Li-ion conductivities. Our study identifies multiple novel chloride systems as fast Li-ion conductors. Given the similarities among halide anion chemistries, our results provide the guidance to tailor cation sublattice for designing novel Li halide SICs.

2. Results

2.1. High-Throughput Computation of Chloride Li-Ion Conductors

From a total of 202 Li-containing chlorides in the ICSD, we selected 20 chloride systems that have fcc and hcp anion frameworks (14 fcc and 6 hcp) with unique cation sublattices (Figure S1 and Table S1, Supporting Information). The selection steps are described in the Experimental Section. In these 20 candidate systems, there are six compositions, $LiMCl_4$, Li_2MCl_4, Li_3MCl_6, $LiMCl_6$, Li_5MCl_8, and Li_6MCl_8, where M is a non-Li metal cation. Examples of crystal structures are shown in **Figure 1**a. In addition, we generated a large number of compounds with different Li contents through aliovalent substitution, which is a common strategy to increase Li-ion conductivities.[24,26] For each materials system, we substituted original M cations by aliovalent elements with different levels of substitutions (e.g., 25%/33%, 50% and 100%) to either create Li-ion vacancies or insert extra Li-ions into empty sites (if available). The doping elements were selected according to valence, ionic radius, and the substitution probability based on Ref. [36] (Experimental Section). The structures of substituted materials were generated following the ordering procedure as in Ref. [26,37,38] (Experimental Section). The energies of these substituted materials were evaluated in density functional theory (DFT) calculations, and the substituted materials with calculated energy above the hull E_{hull} < 40 meV atom^{-1} (**Figure 2** and Table S2, Supporting Information) were further investigated for Li-ion diffusion.

For the candidate materials and their substituted materials with decent phase stability, we performed ab initio molecular dynamics (AIMD) simulations to evaluate their Li-ion conductivities (Table S2, Supporting Information). To identify Li-ion conductors, we employed a screening scheme as in Ref. [26,39], in which we extrapolated the Li-ion conductivities at 300 K using two higher temperatures (500 and 600 K). For the candidates with high extrapolated conductivities at 300 K, we performed AIMD simulations at five temperatures (500, 530, 560, 600, and 650 K) to obtain more accurate Arrhenius relations of Li-ion conductivities on temperature and corresponding activation energies (Figure 2e, Figure S2, and Table S3, Supporting Information). Nineteen materials were identified as potential Li SICs with Li-ion conductivities higher than 1 mS cm^{-1} at 300 K (Figure 2e) with wide electrochemical window (Figure S3, Supporting Information) and large band gaps calculated by DFT hybrid functional calculations (Table S3, Supporting Information). The hypothetical Li_3InCl_6 compound generated by a full In-to-W substitution in the $LiWCl_6$ (*R3*) structure with increased lithium content has an exceptional predicted Li-ion conductivity on the order of 10^{-1} S cm^{-1} at 300 K. Li_3YCl_6 ($P\bar{3}m1$), Li_3ErCl_6 ($P\bar{3}m1$), Li_3InCl_6 (*C2/m*) and Li_3ScCl_6 (*C2/m*) are all confirmed as Li SICs, in agreement with previous experimental reports. Our calculated Li-ion conductivity of Li_3InCl_6 (*C2/m*) is 1.2 mS cm^{-1}, in good agreement with the experimental reported value of 1.49 mS cm^{-1}.[18,21–23] A recent experiment study reports Li-ion conductivity of Li_3YCl_6 to be 0.51 mS cm^{-1}, which is slightly lower than our calculated Li-ion conductivity of 14 mS cm^{-1}, with error bounds in the range of 5 to 47 mS cm^{-1} and the difference may be attributed to the existence of grain boundary[18] and blocking defects.[19] In addition, a wide range of Zr-doped Li_3MCl_6 was reported with greatly enhanced Li-ion conductivity, for example $Li_{5/2}Y_{1/2}Zr_{1/2}Cl_6$ ($P\bar{3}m1$), $Li_{11/4}Sc_{3/4}Zr_{1/4}Cl_6$ (*C2/m*), and $Li_{8/3}Y_{2/3}Zr_{1/3}Cl_6$ ($P\bar{3}m1$). In addition to confirming Li_3MCl_6 as a promising family of Li SICs, these computation results suggest that M^{4+} substitution to create Li vacancies is an effective strategy to further increase the ionic conductivity.

Given that all studied chlorides have close-packed fcc or hcp Cl^- anion sublattices, the differences in Li-ion diffusional properties are mostly a result of different cation configurations

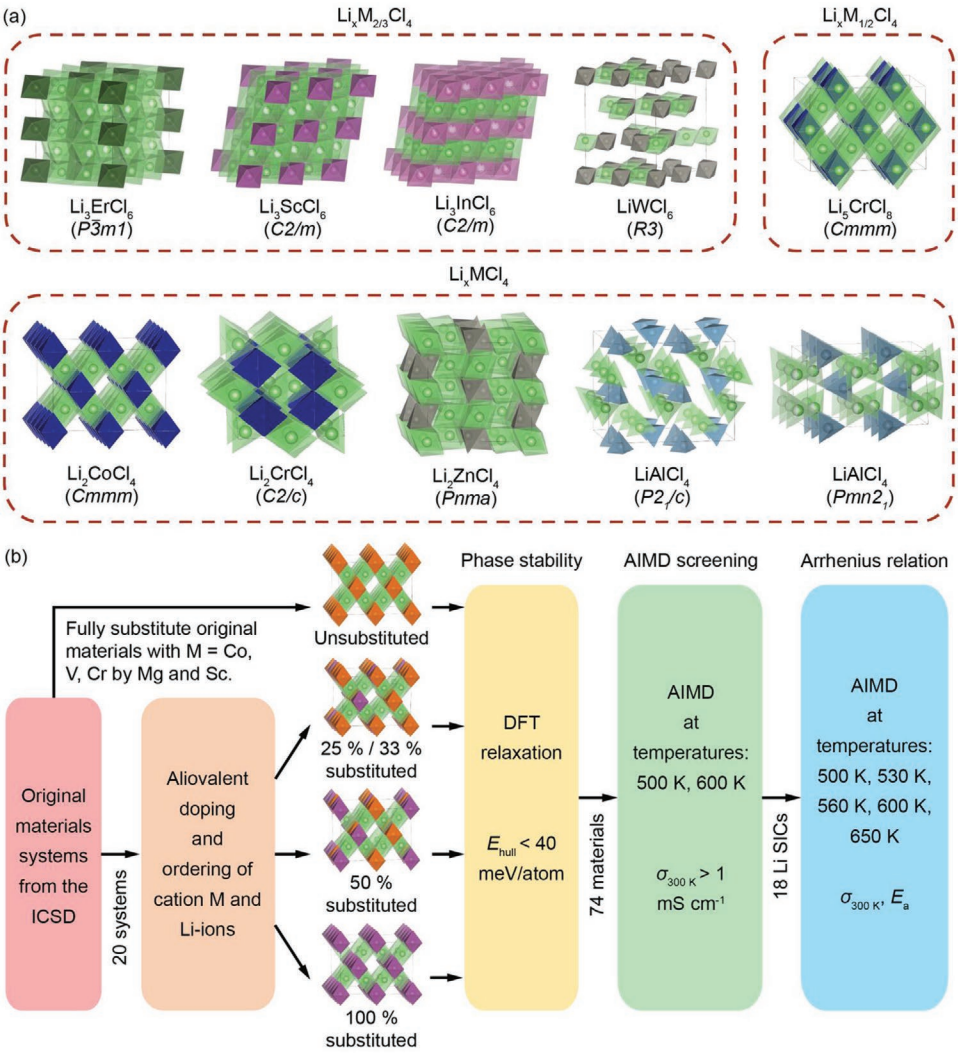

Figure 1. Crystal structures of chlorides and the computation scheme. a) Example crystal structures $Li_xM_{2/3}Cl_4$, $Li_xM_{1/2}Cl_4$, and Li_xMCl_4 materials systems, with $LiCl_6$ octahedra and $LiCl_4$ tetrahedra colored green, and cation MCl_6 octahedra and MCl_4 tetrahedra in different colors. b) The high-throughput computation workflow for studying halide Li-ion conductors.

and Li concentrations. We categorize all materials according to renormalized compositions into Li_xMCl_4 (corresponding to $LiMCl_4$ and Li_2MCl_4), $Li_xM_{2/3}Cl_4$ (corresponding to Li_3MCl_6 and $LiMCl_6$), and $Li_xM_{1/2}Cl_4$ (corresponding to Li_5MCl_8 and Li_6MCl_8), since most known Li-containing chlorides have Li_xMCl_4 compositions. These renormalized compositions allow a straightforward comparison of the concentration of Li-ions and M cations, and the Li-ion diffusional properties vary among different renormalized composition groups. The $Li_xM_{2/3}Cl_4$ materials (i.e., unsubstituted and substituted Li_3MCl_6) in general exhibit the highest Li-ion conductivities (Figure 2). Among all compositions studied, 18 of 28 $Li_xM_{2/3}Cl_4$ materials have Li-ion conductivities higher than 200 mS cm^{-1} at 600 K, while only 4 of 47 Li_xMCl_4 materials and 1 of 11 $Li_xM_{1/2}Cl_4$ materials can achieve a similar level of Li-ion conductivity at 600 K. Among the final 19 identified Li SICs, 16 $Li_xM_{2/3}Cl_4$ materials are identified to have Li-ion conductivity of >1 mS cm^{-1} at RT (Figure 2e). Our results further confirm recent computation and experimental studies that Li_3MCl_6 are promising Li SICs for a wide range of cation and substitutions.[18–25] Most Li_xMCl_4 and $Li_xM_{1/2}Cl_4$ materials even with substantial levels of substitution have Li-ion conductivities much lower than 200 mS cm^{-1} at 600 K, and 24 of 51 materials exhibit a negligible amount of Li-ion hopping to obtain a statistically reliable ionic diffusivity. There are a few Li-ion conductors as the exceptions in the Li_xMCl_4 category, as a result of their distinct local cation coordination, which are further discussed in Section 3.

Our results indicate that the Li content is an important factor for Li-ion conduction. In the fcc and hcp anion sublattices of these materials, the total number of octahedral (oct) sites for Li/M cations is the same as the number of anions N_{Cl}, and the percentile of Li-ions over the oct sites available for Li-ion hopping can be a good quantification for Li content. Here, we define the Li octahedral occupancy $f_{Oct}^{Li} = \frac{N_{Li}}{N_{Cl} - N_M}$ as a ratio of the number of Li-ions N_{Li} over the available oct sites excluding those N_M sites occupied by M cations. As the Li octahedral occupancy f_{Oct}^{Li} decreases, there is an increased number of

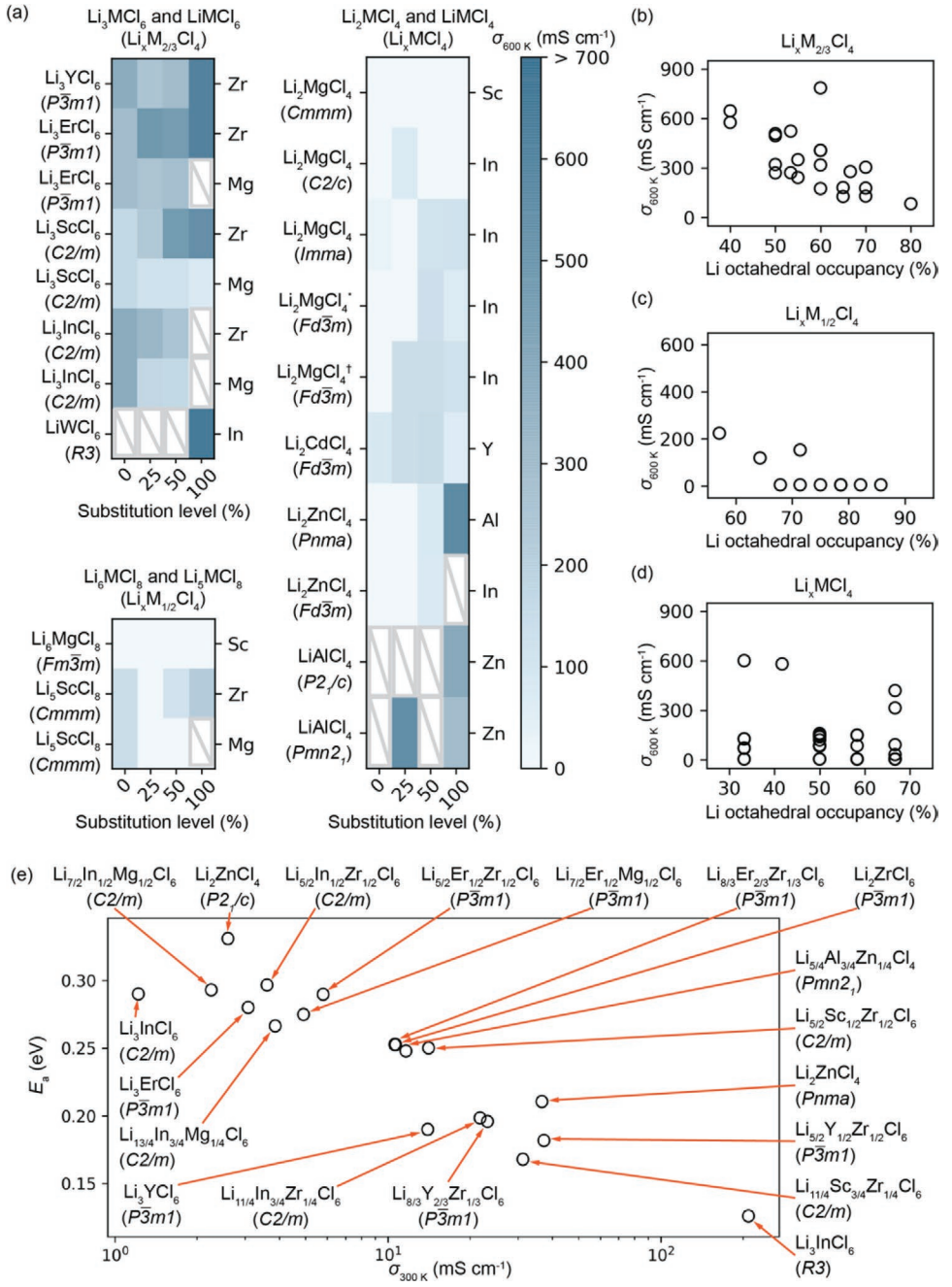

Figure 2. Li-ion conduction in chlorides by ab initio molecular dynamics (AIMD) simulations. a) Li-ion conductivities of Li-containing chlorides at 600 K. Each box in the heatmap corresponds to a compound with the original material (left) substituted by the aliovalent dopant (right) with different substitution levels (For the structures in $P\bar{3}m1$, a substitution level of 1/3 is used instead of 25%), and its Li-ion conductivity at 600 K from AIMD simulations are shown in color. Crossed gray boxes indicate predicted materials with poor phase stability (E_{hull} > 40 meV atom^{-1}) or significant structure change (e.g., melting) during AIMD simulations. Li_2MgCl_4* and $Li_2MgCl_4^{\dagger}$ correspond to ICSD-73229 and ICSD-74957, respectively. Materials are grouped by their renormalized compositions, Li_xMCl_4, $Li_xM_{2/3}Cl_4$, and $Li_xM_{1/2}Cl_4$. Li-ion conductivities versus Li octahedral occupancy in renormalized composition b) $Li_xM_{2/3}Cl_4$, c) $Li_xM_{1/2}Cl_4$, or d) Li_xMCl_4. e) The activation energies E_a and the extrapolated Li-ion conductivities at 300 K of potential Li chloride SICs predicted by the AIMD simulations.

available oct sites for Li-ion hopping, resulting in increased Li-ion conductivity at lower Li octahedral occupancy (Figure 2b–d). In $Li_xM_{2/3}Cl_4$, Li-ion conductivities at 600 K increase with decreasing Li octahedral occupancy f_{Oct}^{Li} until 40% (Figure 2b and S4a, Supporting Information). Among the limited number of materials tested, the materials in $Li_xM_{1/2}Cl_4$ follow a similar trend at 600 K, as a few doped $Li_xM_{1/2}Cl_4$ compositions exhibit higher Li-ion conductivity at low Li octahedral occupancy, and most exhibit low conductivity at higher Li octahedral occupancy (Figure 2c and S4b, Supporting Information). Li-ion

conductivities of $Li_xM_{2/3}Cl_4$ at 500 K have a similar trend of increased Li-ion conduction as Li octahedral occupancy f_{Oct}^{Li} decreases until 50%, and a slight decline of Li-ion conductivity at 500 K occurs when f_{Oct}^{Li} decreases below 50% (Figure S4a, Supporting Information), suggesting an increase in activation energy at low Li octahedral occupancy. In contrast to $Li_xM_{2/3}Cl_4$, Li-ion conductivities of Li_xMCl_4 materials are low across a wide range of Li octahedral occupancies even for highly doped materials (Figure 2d, and S4c, Supporting Information), except for a few exceptions mentioned above. Given the same fcc/hcp anion sublattice in all these materials, the low Li-ion conductivity in Li_xMCl_4 compared to the high Li-ion conductivity in $Li_xM_{2/3}Cl_4$ (i.e., Li_3MCl_6) across a similar range of Li octahedral occupancies can be attributed to different cation concentrations and configurations. Understanding these cation effects on ion conduction is important for guiding the design of novel halide SICs.

2.2. Effect of Cation Sublattice on Li-Ion Migration

To understand the effect of the M cation sublattice on Li-ion diffusion, we performed nudged elastic band (NEB) calculations to evaluate Li-ion migration barriers ΔE_b in 20 materials with different levels of cation substitutions from six representative material systems, Li_6MgCl_8 ($Fm\bar{3}m$), Li_2MgCl_4 ($Cmmm$), Li_2MgCl_4 ($Fd\bar{3}m$), Li_5ScCl_8 ($Cmmm$), Li_3ErCl_6 ($P\bar{3}m1$), and Li_3ScCl_6 ($C2/m$) (Table S5, Supporting Information). In line with the Li-ion conductivities from AIMD simulations, Li-ion migration energies of substituted Li_xMCl_4 (between 0.3 and 0.5 eV) are higher than those in substituted $Li_xM_{2/3}Cl_4$ (between 0.1 and 0.3 eV). For all original unsubstituted materials, the Li-ion migration mediated by a vacancy has an energy barrier on the order of 0.2 eV, which is consistent with the low intrinsic barrier in close-packed Cl^- anion lattice found in previous computation study.[19] However, in unsubstituted Li_xMCl_4 materials, empty octahedron sites for Li-ion migration are blocked by M cations (see *Blocking Effect* in Supporting Information), leading to low ionic conduction in unsubstituted Li_xMCl_4 compounds. Even in the substituted Li_xMCl_4 materials with empty octahedron sites created for Li-ion migration, Li-ion migration barriers ΔE_b increase significantly, consistent with the low Li-ion conductivity in substituted Li_xMCl_4 materials from AIMD simulations (Figure 2). The high energy barriers of Li-ion migration ΔE_b in cation substituted Li_xMCl_4 are caused by increased energy differences between Li sites (**Figure 3**d), which include initial oct, intermediate tetrahedral (tet), and final oct sites, along Li-ion migration pathways. In unsubstituted materials, the site energy differences between initial and final oct sites ΔE_f are almost negligible, leading to low ΔE_b at around 0.2 eV (Figure 3d), and the energy barrier mainly comes from site energy difference between initial oct and intermediate tet sites ΔE_m. In contrast, for substituted Li_xMCl_4 materials, site energy differences ΔE_f increase from 0 eV in unsubstituted materials by 0.05 to 0.4 eV (by 0.18 eV on average), and ΔE_m change by –0.1 to 0.3 eV (by 0.1 eV on average) (Figure S7, Supporting Information), lifting the overall migration barrier ΔE_b to above 0.3 eV. The statistical trends based on a large number of Li-ion migration pathways (Figure 3e,f) confirm that the migration barrier ΔE_b and site energy differences (ΔE_f and ΔE_m) are strongly correlated, and thus increased site energy differences cause increased migration barriers in substituted Li-containing chloride materials.

According to our analyses of the crystal structures of unsubstituted and substituted materials, the increase of site energy differences is caused by the surrounding cation configurations. Unsubstituted materials have low ΔE_f because initial and final oct sites have identical cation environments (Figure 3a,d). However, in partially substituted materials, the cation environments of the initial and final oct sites are different due to the different valence of the substituting cation, causing an increase in the site energy differences (Figure 3b,d). Though fully substituted materials have only a single type of cation, the observed increase in ΔE_f is caused by the change of surrounding Li configurations (Figure 3c,d). In summary, the configurations of cations affect the energies of Li sites and hence the migration barrier.[40,41]

In addition, we performed quantitative analyses of the cation distributions in the structures with high and low energy barriers, which are Li_xMCl_4 and $Li_xM_{2/3}Cl_4$, respectively, to understand the differences in cation sublattice. We analyzed the radial distribution function (RDF) $g(r)$ of all M cations (red curves in Figure 3i–k) and of cations surrounding Li-ions (green curves in Figure 3i–k) on migration paths (Experimental Section), and obtained a range of features (see *Quantitative Analysis of Surrounding Environments* in Supporting Information) describing the cation configuration. We performed a systematic regression analysis of ΔE_f and ΔE_m from many migration pathways on these features of the cation configuration, and the key descriptors are the 2nd M-Li peak in the $g(r)$ of M cations surrounding Li-ions (green curves in Figure 3i–k) and the 1st peak in $g(r)$ of M cation sublattice (red curves in Figure 3i–k). Therefore, compared to the Li_xMCl_4 structures with shorter cation distances, in general, lower cation concentration and sparse cation distribution, such as in $Li_xM_{2/3}Cl_4$, give lower migration barriers even with a substantial level of cation substitution (Figure 3g).

2.3. Tailoring Cation Sublattice for Fast Li-Ion Conduction

We constructed a number of hypothetical chloride materials with reduced cation concentrations to further investigate the effect of cation sublattice on Li-ion conduction. From poor Li-ion conductors Li_2MCl_4 with fcc anion framework, such as Li_2MgCl_4 ($Fd\bar{3}m$), Li_2MgCl_4 ($Imma$), Li_2MgCl_4 ($C2/c$), and Li_2MgCl_4 ($Cmmm$), which have Li-ion conductivities at 600K lower than 80 mS cm^{-1}, we constructed hypothetical $Li_xM_yCl_4$ with higher-valence M^{3+}/M^{4+} cations at reduced concentrations $y = 0.5 - 0.75$, such as $Li_xM_{1/2}Cl_4$, $Li_xM_{5/8}Cl_4$ or $Li_xM_{2/3}Cl_4$, and $Li_xM_{3/4}Cl_4$, (M = Sc^{3+}, Zr^{4+}, Hf^{4+}), in which the M cation sublattice was the same as in Li_2MgCl_4 with a partial occupancy y and the Li content x was adjusted for charge balance following a similar approach used in Section 2.1 (Experimental Section). By comparing the Li-ion conductivities between these hypothetical $Li_xM_yCl_4$ materials and original Li_2MCl_4 materials, we can differentiate how cation concentration and cation configuration (as shown by the $g(r)$ in **Figure 4**c–e) affect Li-ion conduction. The AIMD simulations show that all hypothetical materials with the decreased cation concentration have significantly

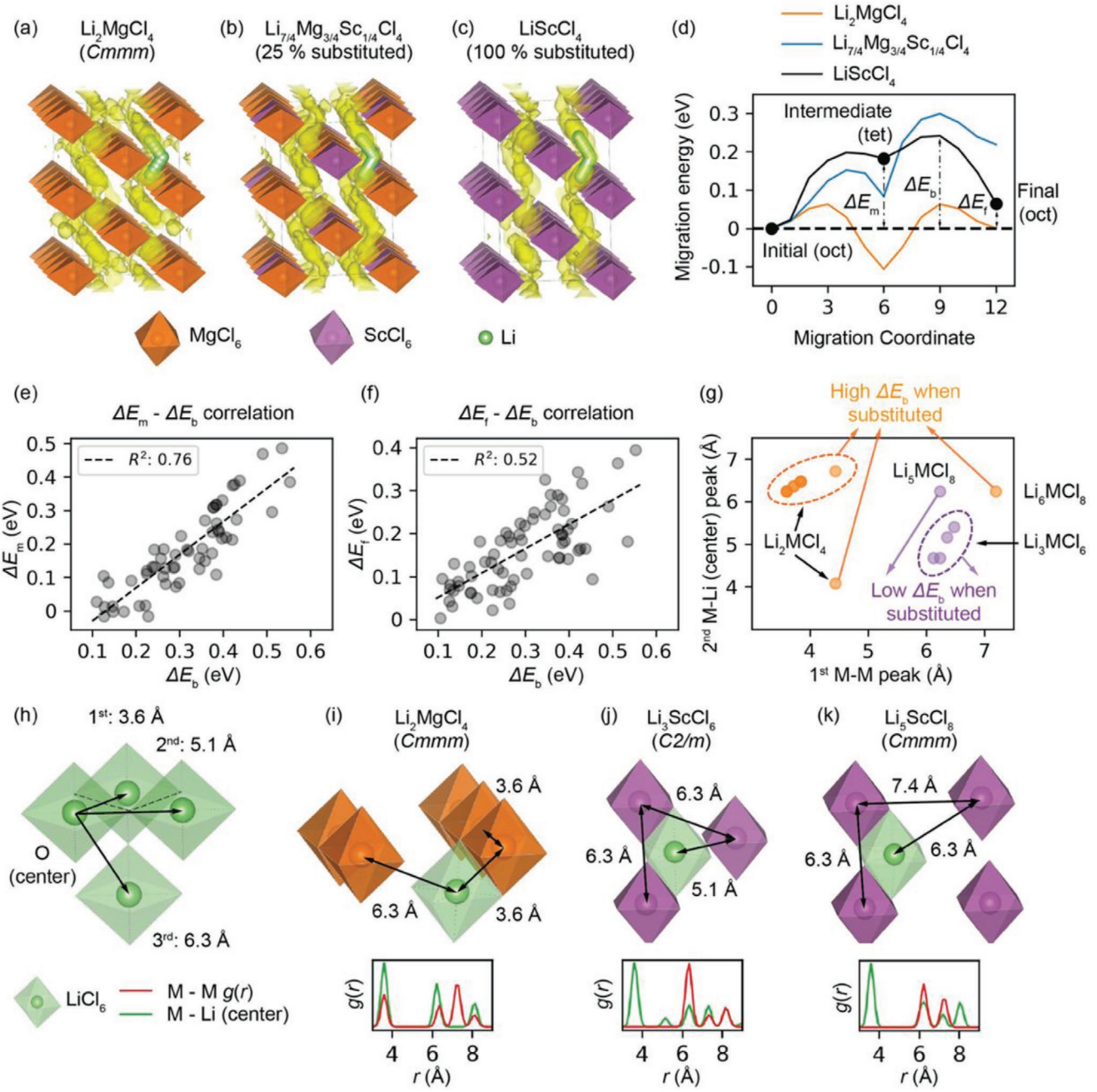

Figure 3. Effect of cation sublattice on Li-ion migration. Li-ion probability density (yellow) from ab initio molecular dynamics (AIMD) simulations at 600 K in crystal structures of a) original, b) 25% Sc-substituted, and c) 100% Sc-substituted Li_2MgCl_4 (*Cmmm*) and Li-ion migration pathways (green) from nudged elastic band (NEB) calculations. d) Energy profile of corresponding migration pathways in a–c) from NEB methods. Correlations between migration energy barrier ΔE_b with site energy differences e) with intermediate site ΔE_m and f) with final site ΔE_f for all migration pathways. g) The 2nd M-Li peak and the 1st M-M peak of RDF $g(r)$ differentiate the materials with high barriers (orange) versus low barriers (purple). h) The configurations of $LiCl_6$ or MCl_6 octahedral sites in fcc Cl^- sublattice in i) Li_2MgCl_4 (*Cmmm*), j) Li_3ScCl_6 (*C2/m*), and k) Li_5ScCl_8 (*Cmmm*), with corresponding RDF $g(r)$ of M cations (red) and M cations surrounding Li centers (green).

increased Li-ion conductivities than the original Li_2MCl_4 materials. A total of 9 of 13 hypothetical Li-ion conductors showed higher Li-ion conductivities of >150 mS cm^{-1} at 600 K compared to those of the original Li_xMCl_4 materials (Figure 4a and Table S6, Supporting Information). All six materials in $Li_xM_{1/2}Cl_4$ and $Li_xM_{5/8}Cl_4$ compositions with most reduced cation concentrations have the Li-ion conductivities near or higher than 200 mS cm^{-1} at 600 K. In agreement with our computation, a recent experimental study of a halospinel material $Li_2Sc_{2/3}Cl_4$ derived from the structure of Li_2MgCl_4 ($Fd\bar{3}m$) achieves high Li-ion conductivity of 1.5 mS cm^{-1} at RT, significantly higher than the original Li_2MgCl_4.[25] The increased

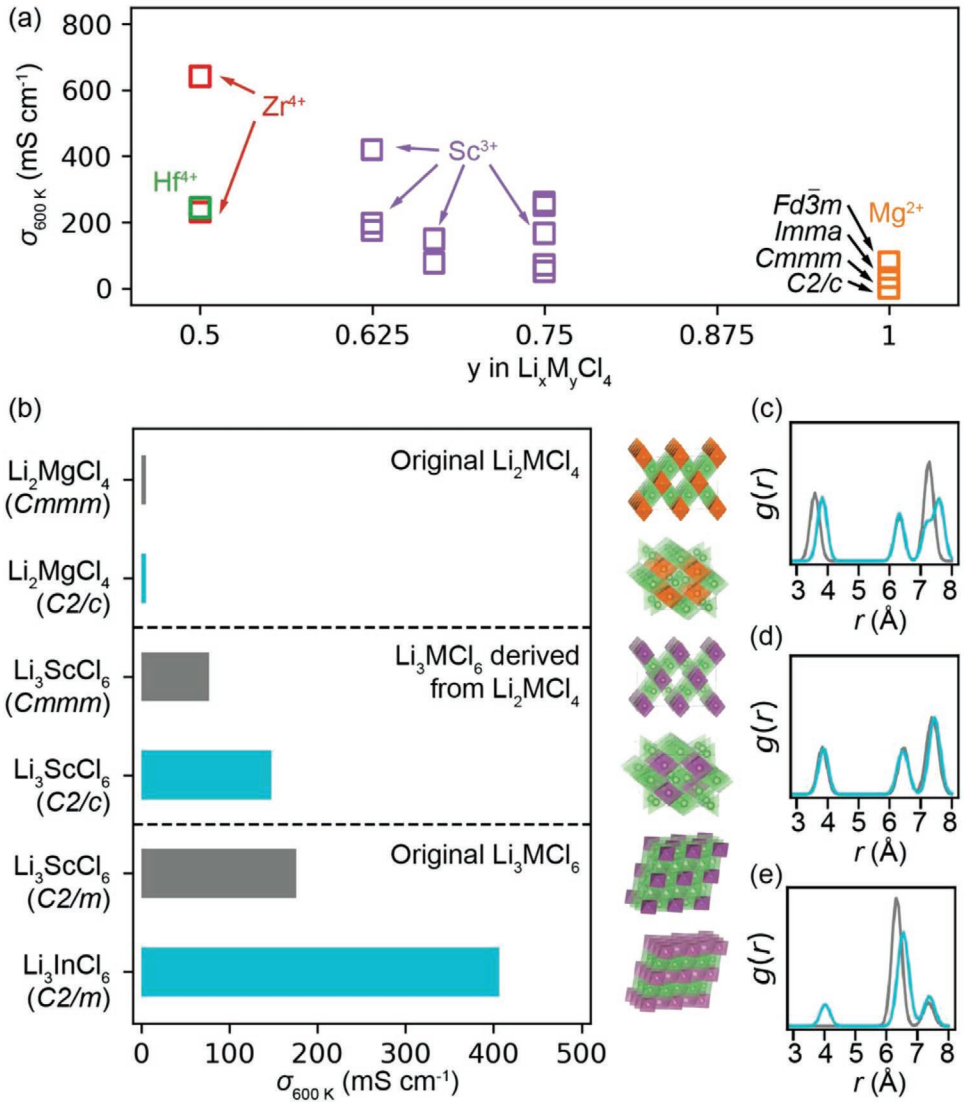

Figure 4. a) Li-ion conductivities at 600 K as a function of M cation concentration *y* in hypothetical Li-ion conductors $Li_xM_yCl_4$, M = Sc^{3+} (purple), Zr^{4+} (red), and Hf^{4+} (green), substituted with reduced M cation concentration from original Li_2MgCl_4 materials (orange). b) Li-ion conductivities at 600 K of (upper) original Li_2MgCl_4, (middle) hypothetical Li-ion conductors derived from Li_2MgCl_4 with reduced cation concentrations, and (lower) original Li_3MCl_6 materials, along with their crystal structures (right) and d–g) RDF *g*(*r*) of M cations.

ionic conductivities of these derived Li-ion conductors with reduced cation concentration in Li_xMCl_4 confirm that low cation concentrations benefits Li-ion conduction in halides.

In addition, we compared materials with identical compositions but different cation configurations, in order to identify the effect of cation configuration on Li-ion conduction. We compared the above two hypothetical Li_3ScCl_6 materials derived from Li_2MgCl_4 with *C2/c* and *Cmmm* space groups, to the original Li_3ScCl_6 (*C2/m*) and Li_3InCl_6 (*C2/m*) (Figure 4b–e), which have highly distinct cation configurations, as indicated by *g*(*r*) and crystal structures in Figure 4. The Li-ion conductivities of our hypothetical Li-ion conductors are around 100 mS cm^{-1} at 600 K, significantly lower than the Li-ion conductivities of existing Li_3MCl_6 materials at 176 and 406 mS cm^{-1} at 600 K. Therefore, original Li_3MCl_6 materials with sparse cation distribution have higher Li-ion conductivities than hypothetical Li_3MCl_6 materials with denser cation distributions derived from poor Li-ion conducting Li_2MCl_4. These results confirm that sparse cation distribution is beneficial for ion conduction in Li-containing chlorides.

3. Discussion and Conclusion

Using first-principles computation, we studied Li-ion conduction in Li-containing chlorides from the ICSD with fcc and hcp anion frameworks. The Li-ion conduction mechanisms were revealed in these materials, with compositions Li_3MCl_6, Li_2MCl_4, and Li_5MCl_8, and their substituted compounds with a wide range of lithium or cation concentrations. By analyzing the trend of Li-ion conductivity among these materials, we revealed that Li content and cation sublattices (including concentration

and distribution) are crucial in determining Li-ion conduction in chloride materials, and the trends with respect to these factors are proposed and demonstrated as design principles for chloride fast Li-ion conductors. Given the similarity among halide anions, these understandings and design principles are expected to be applicable in other halide systems. Among these large number of Li-containing chlorides analyzed, Li-ion conductivities generally increase as Li content decreases, and the optimal Li octahedral occupancy is around 50%, in which Li-ions occupy around half of the octahedral sites excluding M cations and the other half of the sites remain accessible for Li-ion hopping. Our computation confirm Li_3MCl_6 are generally fast Li-ion conductors and have higher Li-ion conductivities than Li_xMCl_4, which tend to have high energy barriers for Li-ion migration in cation-substituted compounds. According to the analyses of a large number of materials, including hypothetically constructed materials, low cation concentration and sparse cation distributions are advantageous for fast Li-ion conduction. Based on the new understanding from our results and analyses, three principles for designing halide Li-ion conductors are 1) decrease Li octahedral occupancy to have a significant fraction of available sites (≈40% to 60%), 2) decrease cation concentrations, and 3) increase cation distances for sparse cation distribution.

Consistent with previous experimental and computational studies, most Li_3MCl_6 materials and their substituted variations are fast Li-ion conductors, as Li_3MCl_6 materials generally satisfy the above principles. According to the above principles, the materials design strategy to further increase the Li-ion conductivity in Li_3MCl_6 is to decrease Li content, which can be accomplished through aliovalent doping by higher valence cations, such as Zr^{4+}. From our computation, substituted Li_3MCl_6 materials such as $Li_{5/2}Y_{1/2}Zr_{1/2}Cl_6$ ($P\bar{3}m1$), $Li_{11/4}Sc_{3/4}Zr_{1/4}Cl_6$ ($C2/m$) and $Li_{11/4}In_{3/4}Zr_{1/4}Cl_6$ ($C2/m$), where M^{3+} are substituted by Zr^{4+}, exhibit high Li-ion conductivities on the level of 10^{-2} S cm^{-1} at RT. These predictions are consistent with recent experimental studies that Li_3MCl_6 (M = Er, Y) substituted by Zr has increased Li-ion conductivity to over 1 mS cm^{-1} at RT.[24] Another recent study on Li_xScCl_{3+x} showed increased cation concentration leads to lower Li-ion conductivity, which is also consistent with our design principle regarding cation concentration.[23] As observed in experiments,[23,24] cation redistribution or reordering may happen in these Li_3MCl_6 systems after substitution, affecting the ion conduction. Given our computation method for materials substitution did not consider these cation redistributions during cation substitution, our computation-predicted Li-ion conductivities may differ from experimental values for some substituted materials, and the effect of Li concentration and cation distribution in substituted Li_3MCl_6 materials merits further study. In summary, our computation study identifies the effect of cation on Li-ion conduction and provides design strategies of tailoring cation distribution and concentrations for fast ion conduction in chlorides. These design strategies are expected to be applicable to other halide systems, indicating further opportunities in designing novel halide SICs with even higher conductivities.

In addition, our computation results also confirm generally low Li-ion conduction in Li_xMCl_4 materials, consistent with earlier experimental studies.[29,30] In contrast to the earlier speculation of poor Li-ion diffusion in close-packed structures,[42,43] first-principles calculations demonstrated that a single Li-ion vacancy in fact has a low barrier in this structure,[19] and the poor Li-ion conductivity in the unsubstituted Li_2MCl_4 is caused by a lack of empty sites, i.e., a low concentration of vacancy sites, which would result in a high activation energy. Our calculations show that certain empty sites are high-energy sites and are unavailable for Li-ion migration in the unsubstituted Li_xMCl_4 materials (see *Blocking Effect* in Supporting Information). While cation-substituted Li_xMCl_4 materials can create more empty sites for Li-ion hopping, they are still poor Li-ion conductors because of greatly increased site energy differences and migration energy barriers. Thus, the poor Li-ion conduction in Li_2MCl_4 is a result of the cation sublattice, rather than the anion sublattice as previously speculated.[42,43] According to our design principles and computation results of hypothetical Li-ion conductors, Li-ion conductivities of Li_xMCl_4 materials can be improved by reducing cation concentrations. Li_xMCl_4 materials with heavily reduced cation concentrations, such as $Li_2Zr_{1/2}Cl_4$ ($C2/c$), $Li_2Zr_{1/2}Cl_4$ ($Cmmm$), and $Li_{17/8}Sc_{5/8}Cl_4$ ($Imma$), have substantially increased Li-ion conductivities (Figure 2). Li_4ZrCl_8 ($Cmmm$), a fully substituted material originating from Li_5CrCl_8 ($Cmmm$), equivalent to $Li_xM_{1/2}Cl_4$ with half the cation concentration of Li_xMCl_4, has considerable Li-ion conduction. A new experimental study on a halospinel $Li_2Sc_{2/3}Cl_4$ ($Fd\bar{3}m$) with reduced cation concentration from Li_2MgCl_4 ($Fd\bar{3}m$) reports greatly increased Li-ion conductivity to 1.5 mS cm^{-1} at RT,[25] confirming our computation predictions and the design principle of reducing cation concentration for increasing Li-ion conduction in Li_xMCl_4 systems. In addition, Li_xMCl_4 systems with different cation site coordination can also lead to higher Li-ion diffusion. From our high-throughput computation, there are a few notable exceptions in substituted Li_xMCl_4 with decent Li-ion conductivity, such as $LiAlCl_4$ ($Pnma$), $Li_{5/4}Al_{3/4}Zn_{1/4}Cl_4$ (Zn-substituted $LiAlCl_4$ ($P2_1/c$)), and Li_2ZnCl_4 (Zn-substituted $LiAlCl_4$ ($Pmn2_1$)), which have cations located on tetrahedral sites instead of on octahedral sites as in other Li_xMCl_4. These materials with cations on tetrahedral sites free octahedral sites for Li-ion migration and open up conduction pathways. A recent experimental study on $LiAlCl_4$ ($P2_1/c$) suggests a Li-ion conductivity of 0.02 mS cm^{-1} at RT, higher than previously reported Li_2MgCl_4 and Li_2CdCl_4, and supports our computation results about potential good Li-ion diffusion in these Li_xMCl_4 systems.[44] Therefore, the strategies for improving ionic conductivity in common Li_xMCl_4 systems are reducing cation concentrations or tailoring cation coordination, which deserve further study.

In conclusion, we systematically studied Li diffusion in a wide range of Li-containing chlorides including a total of 74 compounds derived from 20 known chlorides using first-principles calculations. The high-throughput computation identified and predicted 19 materials as potential Li SICs with Li-ion conductivity of >10^{-3} S cm^{-1} at RT, wide electrochemical window, and large band gaps, as potential SE materials. Our computation on this wide range of chloride materials reveals that Li content and cation sublattice significantly affect Li-ion conduction in Li-containing chloride materials and that low cation concentration and sparse cation distribution are key factors for low Li-ion migration barriers and high Li-ion conductivity. With this

understanding, we propose and demonstrate design principles for increasing Li-ion conductivities of poor Li-ion conductors by artificially altering their cation concentrations and configurations. Our results provide fundamental understanding, new materials systems, and guiding principles to design novel halides as fast Li-ion conductors.

4. Experimental Section

First-Principles Computation: All DFT calculations were performed by using the Vienna ab initio simulation package[45] (VASP) within the projector augmented-wave[46] (PAW) approach. Perdew–Burke–Ernzerhof[47] (PBE) functionals were adopted by generalized-gradient approximation (GGA) to calculate total energies in most of the calculations. In addition, the Heyd–Scuseria–Ernzerhof (HSE) functional[48] was used to calculate the band gap and the density of states (DOS) for potential Li SIC materials. The convergence parameters of all static DFT calculations were consistent with the *Materials Project*.[49,50]

Ab Initio Molecular Dynamics Simulation: AIMD simulations were performed following the same scheme adopted elsewhere.[26] The supercell models for all materials were generated with lattice parameters at around 10 Å or larger. AIMD simulations used nonspin polarized DFT calculations with a Γ-centered 1 × 1 × 1 *k*-point grid. The initial temperature of simulations was set to 100 K after static relaxation of all initial structures. With the time step setting to 2 fs, the structures were heated to the final temperatures at a constant rate by velocity scaling during a period of 2 ps. All simulations adopted the NVT ensemble with Nosé-Hoover thermostat, where an Nosé-mass corresponding to period of 40 time steps was chosen (i.e., SMASS = 0 setting in VASP).[51] The evaluations of ionic diffusivity, conductivity, and corresponding errors followed the method reported elsewhere[52] using the Einstein relation. During the AIMD simulations, the trajectories of all lithium ions were tracked, and the total mean squared displacement (TMSD) of lithium ions was evaluated as a function of time interval Δt as

$$\mathrm{TMSD}(\Delta t) = \sum_{i=1}^{N} \frac{1}{N_{\Delta t}} \sum_{t=0}^{t_{\mathrm{tot}}-\Delta t} \left| \boldsymbol{r}_i(t+\Delta t) - \boldsymbol{r}_i(t) \right|^2 \tag{1}$$

where $\boldsymbol{r}_i$ is the trajectory of the lithium ion i and $N_{\Delta t}$ is the total number of time intervals Δt during the entire time duration t_{tot} of AIMD simulation. TMSD(Δt) is an averaged value of TMSD over all possible time intervals of Δt during the AIMD simulation and represents the total diffusion of all lithium ions over a period of time.

The diffusivity of a specific specie of mobile carrier can be evaluated according to Einstein relation:

$$D = \frac{1}{N} \frac{\mathrm{TMSD}(\Delta t)}{2d\Delta t} \tag{2}$$

where N is the number of the mobile carriers and d is set to 3 for 3D ion conductors. The diffusivity or mobility is defined for a specific species of mobile carrier, for example, Li-ion versus vacancy, and has different values for different mobile carriers, so as the N is different.

The lithium ionic conductivity was calculated following the Nernst–Einstein relation as

$$\sigma = \frac{N}{V} \frac{q^2}{k_{\mathrm{B}}T} D = \frac{q^2}{V k_{\mathrm{B}} T} \frac{\mathrm{TMSD}(\Delta t)}{2d\Delta t} \tag{3}$$

where V is the volume of the model, q is the charge of the carrier, k_{B} is the Boltzmann constant, and T is the temperature. This equation assumes independent hopping of ions, which are confirmed by the AIMD simulations.[19] The calculation of ion conductivity is independent from the choice of specific species of mobile carrier, as the TMSD represents the total diffusion of all lithium ions in the material.

Given that the ion hopping is a stochastic process, the statistical deviations of the diffusivities were evaluated according to the values of TMSD using the scheme reported elsewhere.[52] The total time duration of AIMD simulations were within the range of 100 to 1000 ps until the ionic diffusivity converged with relative standard deviation lower than 25%, which correspond to TMSDs in an approximate range of 2500 to 6000 Å^2. The Li-ion probability density was calculated as the time fraction of Li-ions at each spatial location during the AIMD simulations.[28]

AIMD Screening of Li-Ion Conductors: As an initial screening for fast Li-ion conductors, AIMD simulations were performed at 500 and 600 K in unsubstituted and substituted compounds. The materials with $\sigma_{600\ \mathrm{K}} < 200$ mS cm^{-1} or $\sigma_{500\ \mathrm{K}} < 50$ mS cm^{-1} were first excluded because they were unlikely to be Li SICs at RT. Then materials were selected that satisfy $\log(\sigma T)_{600\ \mathrm{K}} < 1.25\ \log(\sigma T)_{500\ \mathrm{K}} - 0.62$, for which extrapolated Li-ion conductivities are higher than 1 mS cm^{-1} at 300 K. The materials that passed the initial AIMD screening were further evaluated in AIMD simulations at a total of five temperatures (conducting additional simulations at 530, 560, and 650 K) to obtain the Arrhenius relation

$$\sigma T = \sigma_0 \exp\left(-\frac{E_{\mathrm{a}}}{k_{\mathrm{B}}T}\right) \tag{4}$$

where T is temperature, k_{B} is the Boltzmann constant, E_{a} is activation energy, σ_0 is the pre-exponential factor, and σ is conductivity.[26] Using Arrhenius relationship, the activation energy and the evaluated Li-ion conductivity at 300 K were reported.

Nudged Elastic Band Calculations: NEB calculations were performed in the same supercell models. Static relaxation of initial and final structures used an energy convergence criterion at 10^{-7} eV and a force convergence criterion within 0.01 eV Å^{-1}. For NEB calculations, five images were linearly interpolated between the fully relaxed initial and final structures. The energy convergence criterion of NEB calculations was adjusted to 10^{-6} eV and the force convergence criterion was set to 0.05 eV Å^{-1}.

NEB migration pathways were constructed from Li-ion probability density generated by AIMD simulations[28] to best represent the Li-ion hopping with realistic lithium and cation configurations. For unsubstituted compounds with no vacant Li-ion sites, a Li ion was removed from the original structure to create a Li-ion vacancy with a background electron for charge compensation. Two NEB calculations were performed for the first part of migration pathways between initial oct and intermediate tet sites and for the second part between intermediate tet and final oct sites. The energy barrier ΔE_{b} of the complete migration pathway was calculated by the difference between the maximum and minimum energies along the entire oct-tet-oct migration pathway. To have a consistent comparison among different pathways, the initial site was set to the site with the lowest energy, so that ΔE_{f} was equal to or greater than 0 eV.

Selection of Li-Containing Chlorides Systems: The candidate Li-containing chlorides were selected according to the following criteria. Compounds containing H, C, O, S, N, F, Br, I, or radioactive elements or having unbalanced charge were first excluded. From the remaining structures, the anion sublattices with fcc or hcp framework were selected by applying the structural matching algorithm using pymatgen,[53] following a similar scheme.[27] The tolerance parameters of supercell lattice angle and the supercell lattice length were set to 5° and 20%, respectively, and the site root-mean-square tolerance was set to $0.3(V/n)^{1/3}$, where V/n was the volume V normalized by the number of atoms n. One representative compound was kept for each unique structure and distinct cation configuration as a candidate material system. The numbers of compounds that passed each screening step are summarized in Figure S1, Supporting Information.

For candidate systems with redox-active transition metal cations such as Co, Cr, and V, the original cations was first substituted by isovalent nonredox active elements, such as Mg and Sc, as suggested by the ionic substitution probability.[36] For candidate systems with disordered and partially occupied sites, site ordering was performed for these materials following the procedure described below. Then, static DFT relaxations were performed to select the material with the lowest E_{hull}.

Aliovalent Substitution of Materials: The aliovalent substitution elements were identified from the main group elements and Sc, Y, Zr, Zn, and Cd, that have high ionic substitution probability suggested[36] and have ionic radii that satisfy Pauling's first rule.[54]

To obtain substituted materials, 25%/33%, 50%, and 100% of original cations were substituted with a partial occupancy. The Li content of the material was changed accordingly to balance the valence after aliovalent doping. For decreasing Li content, the partial occupancies of original Li-ion sites were correspondingly lowered. For increasing Li content, extra Li-ions were added to empty oct sites with corresponding partial occupancy. The site ordering process was performed to substituted material to obtain the ordered structure with lowest energy. Only materials with good phase stability, i.e., the energies above the hull $E_{hull} < 40$ meV per atom, were kept for further study. For artificially constructed materials with reduced cation concentration in Section 2.3, an identical procedure was followed.

Ordering of Structures with Partial Occupancy: To obtain the ordered structures, 10 000 structures were generated by randomly occupying the disordered sites with probabilities as the corresponding partial occupancies. Among all these structures, 20 symmetrically distinct structures with minimal electrostatic energies were selected for DFT calculations. The structure with the lowest DFT energy was selected as the representative ordered structure for further studies.

Quantitative Analysis of Local Environment Surrounding Cation and Li-Ion: Quantitative analyses of local environments surrounding cation and Li-ion were performed on a large number of individual Li-ion migration pathways. For each individual Li-ion migration pathway, RDFs $g(r)$ of initial, intermediate, and final sites of Li-ion were generated. Two RDFs of surrounding environments for each site, one for surrounding cations and the other one for surrounding Li-ions were generated. The radial distances and coordination numbers obtained from $g(r)$ were used as quantitative features for linear regression models of migration energy barrier and site energy differences (details in Supporting Information).

Supporting Information

Supporting Information is available from the Wiley Online Library or from the author.

Acknowledgements

The authors acknowledge the computational facilities from the University of Maryland supercomputing resources, the Maryland Advanced Research Computing Center (MARCC). Y.M. acknowledges the support from National Science Foundation under award No. 1550423 for the code development of diffusion analyses.

Conflict of Interest

The authors declare no conflict of interest.

Keywords

computational materials discovery, high-throughput computation, Li-ion conductors, super-ionic conductors

Received: July 20, 2020
Revised: August 27, 2020
Published online: September 27, 2020

[1] Z. Zhang, Y. Shao, B. Lotsch, Y. S. Hu, H. Li, J. Janek, L. F. Nazar, C. W. Nan, J. Maier, M. Armand, L. Chen, *Energy Environ. Sci.* **2018**, *11*, 1945.
[2] J. Janek, W. G. Zeier, *Nat. Energy* **2016**, *1*, 16141.
[3] J. Lau, R. H. DeBlock, D. M. Butts, D. S. Ashby, C. S. Choi, B. S. Dunn, *Adv. Energy Mater.* **2018**, *8*, 1800933.
[4] N. Kamaya, K. Homma, Y. Yamakawa, M. Hirayama, R. Kanno, M. Yonemura, T. Kamiyama, Y. Kato, S. Hama, K. Kawamoto, A. Mitsui, *Nat. Mater.* **2011**, *10*, 682.
[5] K. H. Park, Q. Bai, D. H. Kim, D. Y. Oh, Y. Zhu, Y. Mo, Y. S. Jung, *Adv. Energy Mater.* **2018**, *8*, 1800035.
[6] Y. Kato, S. Hori, T. Saito, K. Suzuki, M. Hirayama, A. Mitsui, M. Yonemura, H. Iba, R. Kanno, *Nat. Energy* **2016**, *1*, 16030.
[7] J. C. Bachman, S. Muy, A. Grimaud, H. H. Chang, N. Pour, S. F. Lux, O. Paschos, F. Maglia, S. Lupart, P. Lamp, L. Giordano, Y. Shao-Horn, *Chem. Rev.* **2016**, *116*, 140.
[8] T. Famprikis, P. Canepa, J. A. Dawson, M. S. Islam, C. Masquelier, *Nat. Mater.* **2019**, *18*, 1278.
[9] V. Thangadurai, H. Kaack, W. J. F. Weppner, *J. Am. Ceram. Soc.* **2003**, *86*, 437.
[10] R. Murugan, V. Thangadurai, W. Weppner, *Angew. Chem. Int. Ed.* **2007**, *46*, 7778.
[11] H. Aono, E. Sugimoto, Y. Sadaoka, N. Imanaka, G. ya Adachi, *Solid State Ionics* **1990**, *40-41*, 38.
[12] Y. Zhu, X. He, Y. Mo, *ACS Appl. Mater. Interfaces* **2015**, *7*, 23685.
[13] F. Han, T. Gao, Y. Zhu, K. J. Gaskell, C. Wang, *Adv. Mater.* **2015**, *27*, 3473.
[14] Y. Zhu, X. He, Y. Mo, *J. Mater. Chem. A* **2016**, *4*, 3253.
[15] A. Sakuda, A. Hayashi, M. Tatsumisago, *Chem. Mater.* **2010**, *22*, 949.
[16] J. H. Woo, J. E. Trevey, A. S. Cavanagh, Y. S. Choi, S. C. Kim, S. M. George, K. H. Oh, S.-H. Lee, *J. Electrochem. Soc.* **2012**, *159*, A1120.
[17] Y. Zhu, Y. Mo, *Angew. Chem. Int. Ed.* **2020**, anie.202007621.
[18] T. Asano, A. Sakai, S. Ouchi, M. Sakaida, A. Miyazaki, S. Hasegawa, *Adv. Mater.* **2018**, *30*, 1803075.
[19] S. Wang, Q. Bai, A. M. Nolan, Y. Liu, S. Gong, Q. Sun, Y. Mo, *Angew. Chem. Int. Ed.* **2019**, *58*, 8039.
[20] S. Muy, J. Voss, R. Schlem, R. Koerver, S. J. Sedlmaier, F. Maglia, P. Lamp, W. G. Zeier, Y. Shao-Horn, *iScience* **2019**, *16*, 270.
[21] X. Li, J. Liang, J. Luo, M. Norouzi Banis, C. Wang, W. Li, S. Deng, C. Yu, F. Zhao, Y. Hu, T. K. Sham, L. Zhang, S. Zhao, S. Lu, H. Huang, R. Li, K. R. Adair, X. Sun, *Energy Environ. Sci.* **2019**, *12*, 2665.
[22] R. Schlem, S. Muy, N. Prinz, A. Banik, Y. Shao-Horn, M. Zobel, W. G. Zeier, *Adv. Energy Mater.* **2020**, *10*, 1903719.
[23] J. Liang, X. Li, S. Wang, K. R. Adair, W. Li, Y. Zhao, C. Wang, Y. Hu, L. Zhang, S. Zhao, S. Lu, H. Huang, R. Li, Y. Mo, X. Sun, *J. Am. Chem. Soc.* **2020**, *142*, 7012.
[24] K. H. Park, K. Kaup, A. Assoud, Q. Zhang, X. Wu, L. F. Nazar, *ACS Energy Lett.* **2020**, *5*, 533.
[25] L. Zhou, C. Y. Kwok, A. Shyamsunder, Q. Zhang, X. Wu, L. F. Nazar, *Energy Environ. Sci.* **2020**, *13*, 2056.
[26] X. He, Q. Bai, Y. Liu, A. M. Nolan, C. Ling, Y. Mo, *Adv. Energy Mater.* **2019**, *9*, 1902078.
[27] Y. Wang, W. D. Richards, S. P. Ong, L. J. Miara, J. C. Kim, Y. Mo, G. Ceder, *Nat. Mater.* **2015**, *14*, 1026.
[28] X. He, Y. Zhu, Y. Mo, *Nat. Commun.* **2017**, *8*, 15893.
[29] H. D. Lutz, W. Schmidt, H. Haeuseler, *J. Phys. Chem. Solids* **1981**, *42*, 287.
[30] H. Lutz, Z. Zhang, A. Pfitzner, *Solid State Ionics* **1993**, *62*, 1.
[31] R. Kanno, Y. Takeda, O. Yamamoto, *Mater. Res. Bull.* **1981**, *16*, 999.
[32] C. Catlow, M. Wolf, *Proc. R. Soc. London, Ser. A* **1987**, *413*, 201.
[33] H.-J. Steiner, H. D. Lutz, *Z. Anorg. Allg. Chem.* **1992**, *613*, 26.
[34] L. Kahle, A. Marcolongo, N. Marzari, *Energy Environ. Sci.* **2020**, *13*, 928.

[35] A. M. Nolan, Y. Zhu, X. He, Q. Bai, Y. Mo, *Joule* **2018**, *2*, 2016.
[36] G. Hautier, C. Fischer, V. Ehrlacher, A. Jain, G. Ceder, *Inorg. Chem.* **2011**, *50*, 656.
[37] Q. Bai, X. He, Y. Zhu, Y. Mo, *ACS Appl. Energy Mater.* **2018**, *1*, 1626.
[38] X. He, Y. Mo, *Phys. Chem. Chem. Phys.* **2015**, *17*, 18035.
[39] Z. Zhu, I. H. Chu, S. P. Ong, *Chem. Mater.* **2017**, *29*, 2474.
[40] A. Urban, J. Lee, G. Ceder, *Adv. Energy Mater.* **2014**, *4*, 1400478.
[41] J. Lee, A. Urban, X. Li, D. Su, G. Hautier, G. Ceder, *Science* **2014**, *343*, 519.
[42] S. Hull, *Rep. Prog. Phys.* **2004**, *67*, 1233.
[43] A. Manthiram, X. Yu, S. Wang, *Nat. Rev. Mater.* **2017**, *2*, 16103.
[44] N. Tanibata, S. Takimoto, K. Nakano, H. Takeda, M. Nakayama, H. Sumi, *ACS Mater. Lett.* **2020**, *2*, 880.
[45] G. Kresse, J. Furthmüller, *Phys. Rev. B: Condens. Matter Mater. Phys.* **1996**, *54*, 11169.
[46] P. E. Blöchl, *Phys. Rev. B* **1994**, *50*, 17953.
[47] J. P. Perdew, M. Ernzerhof, K. Burke, *J. Chem. Phys.* **1996**, *105*, 9982.
[48] J. Heyd, G. E. Scuseria, *J. Chem. Phys.* **2004**, *121*, 1187.
[49] A. Jain, G. Hautier, C. J. Moore, S. Ping Ong, C. C. Fischer, T. Mueller, K. A. Persson, G. Ceder, *Comput. Mater. Sci.* **2011**, *50*, 2295.
[50] A. Jain, S. P. Ong, G. Hautier, W. Chen, W. D. Richards, S. Dacek, S. Cholia, D. Gunter, D. Skinner, G. Ceder, K. A. Persson, *APL Mater.* **2013**, *1*, 011002.
[51] S. Nosé, *Prog. Theor. Phys. Suppl.* **1991**, *103*, 1.
[52] X. He, Y. Zhu, A. Epstein, Y. Mo, *npj Comput. Mater.* **2018**, *4*.
[53] S. P. Ong, W. D. Richards, A. Jain, G. Hautier, M. Kocher, S. Cholia, D. Gunter, V. L. Chevrier, K. A. Persson, G. Ceder, *Comput. Mater. Sci.* **2013**, *68*, 314.
[54] L. Pauling, *J. Am. Chem. Soc.* **1929**, *51*, 1010.